

Heterogeneous-free narrow linewidth semiconductor laser with optical injection locking

Author Information

Xiao Sun^{1*}, Zhibo Li¹, Yiming Sun¹, Yupei Wang¹, Jue Wang¹, John H. Marsh¹, Stephen. J. Sweeney¹, Anthony E. Kelly¹, Lianping Hou^{1*}

1. James Watt School of Engineering, University of Glasgow, Glasgow, G12 8QQ, U.K.

* Correspondence: Xiao Sun (Xiao.Sun@glasgow.ac.uk)

James Watt School of Engineering, University of Glasgow
Glasgow, G12 8QQ, U.K
Email: Xiao.Sun@glasgow.ac.uk

* Correspondence: Lianping Hou (Lianping.Hou@glasgow.ac.uk)

James Watt School of Engineering, University of Glasgow
Glasgow, G12 8QQ, U.K
Email: Lianping.Hou@glasgow.ac.uk

Abstract

Narrow-linewidth lasers are indispensable for coherent optical systems, including communications, metrology, and sensing. Although compact semiconductor lasers with narrow linewidths and low noise have been demonstrated, their spectral purity typically relies on hybrid or heterogeneous external-cavity feedback. Here, we present a theoretical and experimental demonstration of a heterogeneous-free optical injection locking (HF-OIL) semiconductor laser. By integrating a topological interface state extended (TISE) laser with a micro-ring resonator (MRR) on an AlGaInAs multiple-quantum-well platform, we achieve monolithic photon injection and phase locking, thereby reducing the optical linewidth. We fabricated and characterized a 1550 nm sidewall HF-OIL laser, achieving stable single-mode operation over a broad current range (65–300 mA) and a side-mode suppression ratio (SMSR) > 50 dB. Under injection locking, the device's Voigt-fitted linewidth narrowed from >1.7 MHz (free-running) to 4.2 kHz, representing a three-order-of-magnitude improvement over conventional distributed-feedback lasers. The intrinsic linewidth of 1.4 kHz is measured by correlated delayed self-heterodyne frequency noise power spectrum density (FN-PSD) method. Moreover, the HF-OIL laser demonstrated high phase stability and

the ability to transition from a random-phased to a phase-locked state. These results underscore the potential of HF-OIL lasers in advancing coherent optical communications and phase encoders in quantum key distribution (QKD) systems.

Introduction

Lasers with high-frequency spectral purity are critical for numerous applications, including sensing and spectroscopy^{1,2}, optical clocks^{3,4}, LIDAR^{5,6}, and microwave photonic devices⁷⁻⁹. Moreover, the demand for low frequency and amplitude noise is paramount in high-data-rate optical communications, particularly in coherent systems¹⁰⁻¹⁴. Although conventional all-solid-state¹⁵ and fiber lasers¹⁶ offer excellent performance, their reliance on discrete, bulky components and low energy conversion efficiency hampers on-chip integration. Semiconductor lasers, by contrast, are more amenable to integration but inherently exhibit linewidths in the MHz range¹⁷, primarily due to their short cavity lengths and limited cavity quality factors is not suitable for the high-speed modulation 16-QAM or 64-QAM requirement (linewidth < 100 kHz).

To address these limitations, prior research has demonstrated that coupling a distributed feedback (DFB) semiconductor laser with a high-Q external optical cavity can create a self-injection-locked (SIL) system. The resulting narrow-band filtering feedback from the external cavity significantly suppresses the laser's phase and frequency noise, thus enhancing its frequency stability. Previous studies have explored various external cavities, such as Fabry-Perot (F-P) etalons^{18,19}, fiber ring resonators²⁰, and whispering-gallery-mode resonators (WGMRs)¹⁷, though these often rely on large-scale fiber-based systems.

For on-chip integration, a common strategy involves hybrid integration of a DFB laser with a micro-ring resonator (MRR) on silicon on insulator (SOI)²¹⁻²³, lithium niobate on insulator(LNOI)²⁴⁻²⁶, and Si₃N₄-based platforms. Si₃N₄²⁷⁻³¹ is widely used to make the external optical cavity due to its low loss, but its footprint is relatively large due to the small refractive index contrast of the Si₃N₄ waveguide. Moreover, phase tuning of Si₃N₄ is mainly based on the thermo-optic effect, which limits the tuning speed to tens of kilohertz³². Rayleigh backscattering in the high-Q (~10⁷) MRR can reduce the laser linewidth to the sub-kHz level. However, under weak feedback conditions (typically <-20 dB), SIL is highly sensitive to the feedback

phase and external perturbations. Moreover, the intensity of Rayleigh backscattered light re-injected into the DFB laser is limited by the coupling efficiency between the DFB device and the external cavity. This coupling is fundamentally limited by the challenges of heterogeneously integrating III-V materials onto silicon platforms. Specifically, achieving effective SIL and external cavity laser (ECL) designs requires high-efficiency coupling components, such as spot size converters (SSCs). Moreover, heterogeneous integration complicates the testing of individual components before their integration into complex systems. This necessitates stringent process control to ensure high yield, while also increasing fabrication complexity and cost.

Sideband Optical injection locking (SOIL) is a technique used to synchronize the frequency and phase of a “slave” laser with an external “master” laser, leveraging photon-photon interactions within the slave cavity³³. Recently, monolithic SOIL (MSOIL) lasers—consisting of two back-to-back distributed feedback (DFB) lasers integrated on chips—have been proposed for high-speed optical communication³⁴⁻³⁶, wavelength proportionality³⁷, and long-distance ranging³⁸. Their adjustable phase characteristics further suggest potential applications in QKD systems³⁹. However, in the back-to-back MSOIL configuration, no compact on-chip optical isolation exists between the master and slave lasers. As a result, the slave’s output light can be reinjected into the master, leading to four-wave mixing and destabilizing the injection-locked state, thus narrowing the operating current range over which stable locking can be maintained⁴⁰. In addition, the cavity quality factor of each sub-laser remains unchanged in this arrangement, thereby limiting the extent of achievable linewidth narrowing in injection locking. Previous research indicates that back-to-back MSOIL lasers maintain a linewidth of 14.88 MHz³⁸ and 2.7 MHz³⁵, comparable to that of conventional DFB lasers. Although injecting an external radio frequency (RF) signal can reduce the laser linewidth to the sub-kHz range^{38,41}, this method requires a low-noise, high-frequency RF source, which limits its practical feasibility.

In this paper, we explore the integration of SIL concepts into the design of monolithic SOIL laser systems. We propose and experimentally demonstrate a heterogeneous-free optical injection locking (HF-OIL)

semiconductor laser configuration by monolithically integrating a topological interface state extended (TISE) laser and an MRR on an AlGaInAs multiple-quantum-well (MQW) platform. The TISE laser configuration establishes a topological interface state at the cavity center, leading to a more uniform photon density distribution and enhancing the optical coupling between the laser and the MRR.

We fabricated a sidewall HF-OIL laser with a single-mode locking operation DFB current range from threshold 65 mA to 300 mA, and a side mode suppression ratio (SMSR) above 50 dB even without anti-reflection (AR) facet coatings. Under injection locking, the intrinsic linewidth narrows significantly from 2 MHz to 4.2 kHz compared to the free-running state. The footprint of HF-OIL laser is only about $1000 \times 0.2 \mu\text{m}^2$, much smaller than the hybrid Si_3N_4 or SOI SIL/ECL laser. We also present a proof-of-concept demonstration using the coherent-one-way (COW) protocol to modulate the HF-OIL laser, illustrating its superior phase stability. Furthermore, a phase-switching modulation experiment confirms the device's ability to transition from a random-phase state to a phase-locked state, effectively toggling between locked and unlocked conditions. This HF-OIL system achieves superior single-mode, small footprint, narrow-linewidth performance without relying on a hybrid external cavity. Its fabrication is also simplified, requiring only a single metalorganic vapor-phase epitaxy (MOVPE) growth and one inductively coupled plasma (ICP) dry etching step. These results highlight the potential of the HF-OIL laser for integrated photonic platforms, offering improved stability, reduced complexity, and enhanced performance for coherent optical systems and phase encoder ability in QKD systems.

Results

Design of the HF-OIL laser

The traditional π -phase shifted uniform Bragg grating is shown in Fig. 1a. This structure consists of two Bragg reflection mirrors with a π -phase shift between them. Figure 1b presents the structure of the TISE laser, which includes left and right reflection uniform grating mirrors (L_{LG} and L_{RG}) with inversion symmetry, and a central topological interface state extending (TISE) cavity (L_M). Here, A_M is the lateral

modulation period and Λ denotes the cell period. The modulation process in the TISE cavity is shown in Fig. 1c, where Λ is the Bragg grating period, n_1 and n_2 refer to two different refractive index segments. The positions of the n_1 and n_2 are changed with a shift step $\Delta\Lambda$ while maintaining a constant Λ during each modulation cycle. Within the modulation period Λ_M , an alignment factor, $\Delta\Lambda$ quantifies the adjustment of the phase shift step across each sampling period Λ_M . After a lateral modulation period Λ_M , the cell returns to the initial state, resulting in $\Delta\Lambda = \Lambda$. For a lateral modulation period Λ_M with n^{th} modulation, it holds that $\Lambda_M = n\Lambda$. The TISE cavity contains N number of Λ_M and the total length of TISE (L_M) is equal to $N\Lambda_M$. Figure 1d illustrates, from left to right, the calculated 1D band structures of the left grating, the TISE cavity, and the right grating. Both the left and right gratings exhibit two Zak phase inversion centers, while the energy band in the TISE cavity is degenerate.

Figure 1e illustrates the structure of the HF-OIL laser, which integrates a TISE laser with an MRR on an AlGaInAs MQW platform which the gain peak center is around 1560 nm (see Supplementary Part A). The TISE laser, measuring 1000 μm in total length, comprises symmetrically inverted left and right reflective grating mirrors (450 μm each) flanking a central TISE cavity (100 μm) as shown in Figure 1f. The band-degenerated TISE cavity provides topological protection of the phase transition between the left and right gratings, thereby enabling the topological interface state (TIS) mode to extend uniformly across the cavity's center.

At the cavity midpoint, a 150 μm radius MRR is integrated close to the TISE cavity. Depending on our calculation result (see Supplementary Part A), for $R > 150\mu\text{m}$, the increase in the Q factor is minimal, further increasing R does not significantly improve the linewidth narrowing effect. As light propagates through the TISE laser, a portion of light is coupled into the MRR. After resonant circulation within the MRR, this light is re-injected into the TISE laser, achieving optical injection locking. Due to the structural asymmetry, the MRR can couple simultaneously to both left-propagating (green arrow) and right-propagating (red arrow) modes in the TISE laser cavity. Figures 1g and 1h show the transmission spectrum and normalized photon distribution of the TISE laser, compared against a conventional π -phase shift DFB laser. The results indicate that the TISE cavity effectively suppresses side modes and produces a more

uniform field distribution at the waveguide center. This uniformity enhances the coupling efficiency between the TISE laser and the MRR. Figures 1i show the transmission spectrum from the MRR to the TISE laser and the quality factor $Q = 1.1 \times 10^5$. The efficiency of injection locking can be described by an equation derived for the reduction of the close-in linewidth of the laser (see Supplementary Part B).

$$\delta \approx \frac{P_r}{P} (1 + \alpha_H^2) \left(\frac{Q_{MRR}}{Q_{LD}} \right)^2 \quad (1)$$

Where P_r is the feedback power from the MRR, and P is the TISE laser power. Q_{LD} represents the quality factor of laser, while Q_{MRR} denotes the quality factor of MRR, α_H is the linewidth enhancement factor. By substituting reasonable numbers in equation (1) for $P_r/P = 0.03$, $\alpha_H = 3$, $Q_{MRR} = 1.1 \times 10^5$, and $Q_{LD} = 4 \times 10^3$, we find that the laser linewidth can be improved by a factor of 225. The locking range is defined as the frequency range over which the TISE laser emission injection locks to the MRR resonance and follows the expression:

$$\Delta f_{lock} \approx \sqrt{\frac{P_r}{P} (1 + \alpha_H^2)} \frac{f_0}{Q_{LD}} \quad (2)$$

Where f_0 represents centre frequency of the laser. The theoretically estimated locking range $\Delta f_{lock} \approx 26$ GHz.

Experiment

The devices were fabricated on an AlGaInAs/InP epitaxial structure featuring five quantum wells (QWs) and six quantum barriers, with a QW confinement factor of 5%⁴². The room-temperature photoluminescence (PL) wavelength of the QWs was set to 1530 nm. A scanning electron microscope (SEM) image of the HF-OIL laser is shown in Fig. 2a. The grating ridge waveguide was designed with a width of 2.0 μm , a sidewall corrugation depth of 300 nm, and a ridge height of 2.0 μm . The minimum gap between the MRR and the TISE laser was maintained at 300 nm.

The laser chip was mounted on a thermoelectric cooler (TEC) set to 20°C to mitigate long-term drift. The MRR is also carrier injected to reduce the internal absorption loss of the MQW. Figure 2b shows the typical current–power (I_{TISE} - P) characteristics of the TISE laser under different MRR injection currents (I_{MRR}). The threshold current is approximately 65 mA, and the slope efficiency is about 0.07 W/A. Notably, varying I_{MRR} has only a minor influence on the TISE laser’s output power. At $I_{MRR} = 300$ mA, the saturation power is slightly reduced compared to $I_{MRR} = 150$ mA, likely due to increased cavity temperature resulting from the higher injection current. The laser is still able to deliver power up to 11 mW. Figure 2c compares the optical spectra of the laser in its injection-locked and free-running states. Under injection locking, the spectral linewidth is notably narrowed, and the side-mode suppression ratio (SMSR) exceeds 50 dB. To examine the locking state range, we fixed I_{TISE} at 200 mA and varied I_{MRR} from 100 mA to 300 mA, as shown in Figure 2d. Once I_{MRR} surpasses 171 mA, the spectrum transitions from a broad (free running) to a narrow (locked) linewidth, defining a locking range from 171 mA to 300 mA. The current-induced wavelength redshift coefficient (ACWRC) of the I_{MRR} is found at 0.01022 nm/mA. Figures 2e–f present 2D spectral maps of the laser for I_{TISE} values ranging from its threshold to 300 mA, at $I_{MRR} = 0$ mA, 150 mA, and 300 mA. The ACWRC for the I_{TISE} is 0.01038 nm/mA, indicating that the wavelength redshift coefficient for TISE laser injection (with the I_{MRR} fixed) closely matches that of MRR laser injection (with the I_{TISE} fixed). As a result, the TISE laser and MRR exhibit excellent wavelength tuning synchronization, enabling a wide injection-locked range. These results confirm that the HF-OIL laser remains in the injection-locked state over a wide current range, maintaining stable locking for I_{TISE} from threshold to 300 mA when $I_{MRR} = 300$ mA.

Then we investigated the coherence properties of the HF-OIL laser. The laser linewidth was measured using a fiber-delayed, non-zero frequency delayed self-heterodyne (DSH) method, employing a 25-km single-mode fiber delay and an 80-MHz acoustic-optic modulator (AOM), as shown in Fig. 3a. A comparison of the free-running and injection-locked states is presented in Fig. 3b, revealing a pronounced linewidth narrowing under injection locking. Voigt fitting of the spectra is shown in Fig. 3c. Since the Gaussian noise

has a more prominent effect on broadening the spectral line near the center⁴³, the intrinsic Lorentzian linewidth is estimated by measuring the -20 dB bandwidth and applying a $2\sqrt{99}$ division factor to reduce the effect of Gaussian noise⁴⁴. Stable injection locking is obtained with an intrinsic Lorentzian linewidth of 4.2 kHz. We further examined the linewidth variation as a function of I_{TISE} and compared it to the free-running state, as illustrated in Fig. 3d. Under free-running conditions, the intrinsic linewidth ranged from 1.7 MHz to 3.6 MHz, whereas injection locking reduced it to 4.2 kHz to 13 kHz—an improvement by a factor greater than 250 , which is corresponded to the calculated reduction of the close-in linewidth factor. The linewidth is < 8 kHz within the I_{TISE} range of $140 - 260$ mA. Figure 3e shows the linewidth reduction as I_{MRR} increases, with the laser transitioning from the free running to the locked state.

To confirm the linewidth, we employed the correlated delayed self-heterodyne frequency noise power spectrum density (FN-PSD) method (details in Methods). The recorded frequency noise is displayed in Fig. 3f. A white noise floor of approximately 446 Hz²/Hz is observed, which corresponds to an intrinsic linewidth (Lorentzian linewidth) of 1.4 kHz for the laser. This further confirms the narrow-linewidth performance of the laser in the locked state, in contrast to the free-running state, where the intrinsic linewidth is 2.6 MHz.

We evaluated the coherence of successive pulses in a pulse train under two optical injection conditions: a continuous wave (CW) MRR and a directly modulated MRR. The measurement setup, depicted in Fig. 4a, is based on an asymmetric Mach–Zehnder interferometer (AMZI). A thermal phase modulator (PM) in the short arm controls the relative phase between the two arms, while an acoustic-optic modulator (AOM) introduces an 80 MHz frequency shift. This shift facilitates the differentiation of low-frequency electronic noise from the beat signal on the PD, thus improving measurement accuracy and signal-to-noise ratio.

The TISE laser is driven by a 5 MHz RF signal with voltage of peak to peak at 400 mV, and the AMZI is configured with a 200 ns delay between its short and long arms—matching the 200 ns interval between consecutive pulses at 5 MHz (Fig. 4b). Under the CW-locked MRR condition, as illustrated in Fig. 4c, each pulse inherits the coherence from the locking process, and the phase difference between consecutive pulses

remains fixed. This behavior closely mimics the saturation regime of the COW protocol. Conversely, when the MRR is directly modulated and the TISE laser operates in CW mode, the HF-OIL laser cycles between phase-locked and random-phase states, causing the phase of consecutive pulses to vary and no longer remain fixed.

Discussion

The concept of injection locking—recently employed in narrow-linewidth semiconductor lasers through heterogeneous integration of III–V gain media and ultra-high-Q silicon-based microresonators—has been extensively explored for coherent optical systems. In contrast to heterogeneous approaches, monolithic integration unifies the material platform, reducing the device footprint, fabrication complexity and cost. However, most monolithic semiconductor lasers exhibit linewidth on the order of megahertz.

In this work, we present a heterogeneous-free HF-OIL laser fabricated on an InP platform. This device combines an MRR with a quality factor of 10^5 and a novel TISE laser. The TISE laser employs a mode-extension cavity that expands the fundamental optical mode from the cavity center to its edges, producing a uniform photon density distribution at the cavity center and thereby enhancing its coupling efficiency to the MRR.

Our measurements show that the injection-locked HF-OIL laser achieves an Voigt-fitted linewidth of 4.2 kHz, FN-PSD linewidth 1.4 kHz more than 200 times narrower than its free-running state. Table 1 compares the performance of our HF-OIL laser with various hybrid and monolithic III-V narrow-linewidth semiconductor lasers. Notably, our device achieves a significantly narrower linewidth than typical monolithic III–V lasers, with performance on par with hybrid self-injection-locked and external-cavity lasers. The fabrication process of HF-OIL laser is also the simplest, with only one step of MOVPE epitaxial growth and one step ICP dry etch. Additionally, our experiments demonstrate the intrinsic phase-adjustment capability of the HF-OIL laser, highlighting its potential for both quantum and conventional coherent communication systems. This intrinsic phase control also enables the seamless combination of QKD and high-bandwidth data transmission, underscoring the versatility and promise of the HF-OIL laser platform.

Table 1 Performance comparison of hybrid integrated SIL/ECL lasers and other narrow-linewidth DFB/DBR lasers in the 1550 nm.

Reference	Structure	Power (mW)	SMSR (dB)	Linewidth (kHz)
22 (2018)	Si-Hybrid ECL	11	> 46	37 (FN-PSD)
45 (2021)	Si-Hybrid ECL	> 2	> 40	105 (FN-PSD)
46 (2024)	Si-Hybrid ECL	16.4	> 45	2.79 (DSH)
21 (2022)	Si-Hybrid filter/SIL	> 2	> 40	27 (FN-PSD)
23 (2023)	Si-Hybrid ECL	76	> 50	12 (FN-PSD)
47 (2020)	SiN-Hybrid ECL	0.5	> 55	4 (FN-PSD)
48 (2021)	SiN-Hybrid SIL	37.9	56	3 (FN-PSD)
25 (2022)	LNOI-Hybrid ECL	3.7	> 50	15 (DSH) / 11.3 (FN-PSD)
49 (2024)	LNOI-Hybrid SIL	0.74	/	45.5 (DSH)
50 (2024)	LNOI-Hybrid SIL	3.18	60	2.5 (FN-PSD)
51 (2015)	InP-DBR Butt joint	> 120	> 50	70 (FN-PSD)
52 (2022)	InP-QW DFB	45	58.7	63 (DSH)
53 (2022)	InP-DBR Butt joint	18	54	45 (DSH) /10 (FN-PSD)
54 (2019)	InP-QW DFB	/	/	100 (DSH)
This Work	InP-QW HF-OIL	11	> 50	4.2 (DSH) /1.4 (FN-PSD)

Methods

Device fabrication

The fabrication procedure for the HF-OIL laser can be found in Supplementary Part C. The wafer was grown on an InP substrate using MOVPE. The room temperature photoluminescence (PL) peak of the QWs was located at a wavelength of 1530 nm. The TISE laser sidewall grating and MRR waveguide was defined by electron-beam lithography (EBL) on an EBPG5200 E-beam system, with negative-tone Hydrogen Silsesquioxane (HSQ) acting as both the EBL resist and a hard mask for ICP dry etching using a $\text{Cl}_2/\text{CH}_4/\text{H}_2$ gas mixture in an Oxford PlasmaPro 300 system. Subsequent steps included PECVD deposition of SiO_2 (Oxford PlasmaPro 100 PECVD), application of HSQ passivation layers, SiO_2 window opening, P-contact deposition, substrate thinning, and N-contact deposition, all performed using conventional laser diode fabrication techniques. These two micro electrodes only require one step of lithography together with the large area electrode pads. Scanning electron microscopy images were acquired using a Hitachi SU8240 scanning electron microscope operating at 100 kV.

Measurement setup

The laser was driven by a continuous-wave current source (Newport Model 8000). An isolator was placed at the laser output. The light passed through the isolator and entered coupler 1, which had a splitting ratio of 50:50, dividing the light into two paths. One path included a time-delay fiber and a polarization controller (FPC032), while the other path included an 80-MHz acoustic-optic modulator (Aerodiode 1550-AOM). These two paths were then combined in coupler 2 and split again into two paths: one leading to a photodetector (Thorlabs DET08CFC) and the other to an optical spectrum analyzer (Agilent 86140B). Both the current driver and the electronic spectrum analyzer (Keysight N9000B) were controlled by a computer via the general-purpose interface bus (GPIB) interface using LabVIEW software. For the correlated delayed self-heterodyne FN-PSD method, the experimental setup is similar to the one shown in Fig. 3a, with the key difference being a 40 m long fiber line to delay the optical path.

The phase encoding experiment is conducted using the setup shown in Fig. 4a. A phase modulator (Thorlabs LNP6118) maintains the phase difference between the two AMZI paths, while the signal is analyzed with a real-time oscilloscope (Keysight UXR0334A).

Data Availability

The data that support the findings of this study are available from the corresponding author upon reasonable request.

Acknowledgment

The authors would like to thank the staff of the James Watt Nanofabrication Centre (JWNC) at the University of Glasgow for their help in fabricating the devices. The author sincerely thanks Rachel Love in the assistance in JWNC and the Critical Technologies Accelerator for support of this research.

References

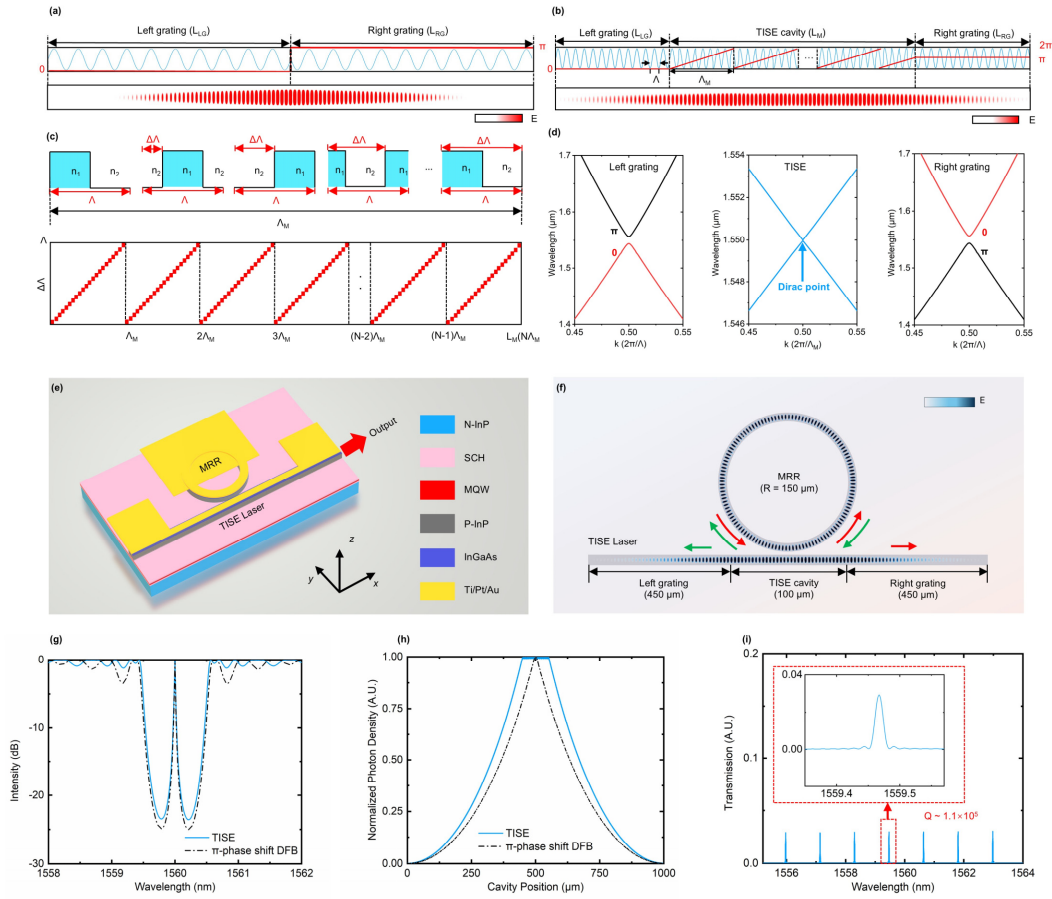
- 1 Luvsandamdin, E. *et al.* Micro-integrated extended cavity diode lasers for precision potassium spectroscopy in space. *Opt. Express* **22**, 7790-7798 (2014).
- 2 Suh, M.-G., Yang, Q.-F., Yang, K. Y., Yi, X. & Vahala, K. J. Microresonator soliton dual-comb spectroscopy. *Science* **354**, 600-603 (2016).
- 3 Katori, H. Optical lattice clocks and quantum metrology. *Nat. Photonics* **5**, 203-210 (2011).

- 4 Newman, Z. L. *et al.* Architecture for the photonic integration of an optical atomic clock. *Optica* **6**, 680-685 (2019).
- 5 Trocha, P. *et al.* Ultrafast optical ranging using microresonator soliton frequency combs. *Science* **359**, 887-891 (2018).
- 6 Suh, M.-G. & Vahala, K. J. Soliton microcomb range measurement. *Science* **359**, 884-887 (2018).
- 7 Liu, J. *et al.* Photonic microwave generation in the X-and K-band using integrated soliton microcombs. *Nat. Photonics* **14**, 486-491 (2020).
- 8 Marpaung, D., Yao, J. & Capmany, J. Integrated microwave photonics. *Nat. Photonics* **13**, 80-90 (2019).
- 9 Liang, W. *et al.* High spectral purity Kerr frequency comb radio frequency photonic oscillator. *Nat. Commun* **6**, 7957 (2015).
- 10 Jin, W. *et al.* Hertz-linewidth semiconductor lasers using CMOS-ready ultra-high-Q microresonators. *Nat. Photonics* **15**, 346-353 (2021).
- 11 Xiang, C. *et al.* 3D integration enables ultralow-noise isolator-free lasers in silicon photonics. *Nature* **620**, 78-85 (2023).
- 12 Guo, J. *et al.* Chip-based laser with 1-hertz integrated linewidth. *Science advances* **8**, eabp9006 (2022).
- 13 Fan, Y. *et al.* Hybrid integrated InP-Si₃N₄ diode laser with a 40-Hz intrinsic linewidth. *Opt. Express* **28**, 21713-21728 (2020).
- 14 Xiang, C., Jin, W. & Bowers, J. E. Silicon nitride passive and active photonic integrated circuits: trends and prospects. *Photonics Research* **10**, A82-A96 (2022).
- 15 Qiao, S. *et al.* Ultra-highly sensitive dual gases detection based on photoacoustic spectroscopy by exploiting a long-wave, high-power, wide-tunable, single-longitudinal-mode solid-state laser. *Light-sci Appl* **13**, 100 (2024).
- 16 Ruan, Q. *et al.* Visible - Wavelength Spatiotemporal Mode - Locked Fiber Laser Delivering 9 ps, 4 nJ Pulses at 635 nm. *Laser & Photonics Reviews* **16**, 2100678 (2022).
- 17 Liang, W. *et al.* Ultralow noise miniature external cavity semiconductor laser. *Nat. Commun* **6**, 7371 (2015).
- 18 Savchenkov, A., Zhang, W., Iltchenko, V. & Matsko, A. Robust self-injection locking to a non-confocal monolithic Fabry–Perot cavity. *Opt. Lett.* **49**, 1520-1523 (2024).
- 19 Pericherla, S. V., Trask, L., Shirpurkar, C., Bhardwaj, A., Hoefler, G. E. & Delfyett, P. J. Stabilization of an InP Mode-Locked Laser PIC Through Simultaneous Optical Filtering and Self-Injection Locking Using a Fabry-Perot Etalon. *J. Lightwave Technol.* (2024).
- 20 Spirin, V. V., Bueno Escobedo, J. L., Korobko, D. A., Mégret, P. & Fotiadi, A. A. Stabilizing DFB laser injection-locked to an external fiber-optic ring resonator. *Opt. Express* **28**, 478-484 (2020).
- 21 Aihara, T. *et al.* Heterogeneously integrated widely tunable laser using lattice filter and ring resonator on Si photonics platform. *Opt. Express* **30**, 15820-15829 (2022).
- 22 Guan, H. *et al.* Widely-tunable, narrow-linewidth III-V/silicon hybrid external-cavity laser for coherent communication. *Opt. Express* **26**, 7920-7933 (2018).
- 23 Li, C., Sui, S., Gao, F., Wang, Y., Xu, X. & Zhao, J. High-power III-V/Si integrated wavelength tunable laser for L-band applications. *IEEE Journal of Quantum Electronics* (2023).
- 24 Li, Z. *et al.* High density lithium niobate photonic integrated circuits. *Nat. Commun* **14**, 4856 (2023).

- 25 Li, M. *et al.* Integrated pockels laser. *Nat. Commun* **13**, 5344 (2022).
- 26 Zhang, M., Wang, C., Cheng, R., Shams-Ansari, A. & Lončar, M. Monolithic ultra-high-Q lithium niobate microring resonator. *Optica* **4**, 1536-1537 (2017).
- 27 Lihachev, G. *et al.* Low-noise frequency-agile photonic integrated lasers for coherent ranging. *Nat. Commun* **13**, 3522 (2022).
- 28 Su, Q. *et al.* A self-injection locked laser based on high-Q micro-ring resonator with adjustable feedback. *J. Lightwave Technol.* (2023).
- 29 Prokoshin, A., Gehl, M., Madaras, S., Chow, W. W. & Wan, Y. Ultra-narrow-linewidth hybrid-integrated self-injection locked laser at 780 nm. *Optica* **11**, 1024-1029 (2024).
- 30 Voloshin, A. S. *et al.* Dynamics of soliton self-injection locking in optical microresonators. *Nat. Commun* **12**, 235 (2021).
- 31 Wildi, T., Ulanov, A. E., Voumard, T., Ruhnke, B. & Herr, T. Phase-stabilised self-injection-locked microcomb. *Nat. Commun* **15**, 7030 (2024).
- 32 Guo, Y. *et al.* Thermally tuned high-performance III-V/Si₃N₄ external cavity laser. *IEEE Photonics Journal* **13**, 1-13 (2021).
- 33 Liu, Z. & Slavík, R. Optical injection locking: From principle to applications. *J. Lightwave Technol.* **38**, 43-59 (2020).
- 34 Kasai, K., Wang, Y., Beppu, S., Yoshida, M. & Nakazawa, M. 80 Gbit/s, 256 QAM coherent transmission over 150 km with an injection-locked homodyne receiver. *Opt. Express* **23**, 29174-29183 (2015).
- 35 Zhang, Y. *et al.* Experimental demonstration of single sideband modulation utilizing monolithic integrated injection locked DFB laser. *J. Lightwave Technol.* **38**, 1809-1816 (2020).
- 36 Zhang, Y. *et al.* Modulation properties enhancement in a monolithic integrated two-section DFB laser utilizing side-mode injection locking method. *Opt. Express* **25**, 27595-27608 (2017).
- 37 Wang, L. *et al.* Highly-reflective facet-coated multi-wavelength DFB laser array with exact wavelength spacings. *Opt. Express* **32**, 1843-1850 (2024).
- 38 Zhang, Y. *et al.* Monolithic integrated linear frequency modulated dual-wavelength DFB laser chip with high linearity and its application in long distance ranging. *ACS Photonics* **10**, 2344-2352 (2023).
- 39 Paraíso, T. K. *et al.* A modulator-free quantum key distribution transmitter chip. *npj Quantum Information* **5**, 42 (2019).
- 40 Fan, Y., Zhang, Y., Sun, Y., Yuan, B., Marsh, J. H. & Hou, L. in *The European Conference on Lasers and Electro-Optics*. cb_p_3 (Optica Publishing Group).
- 41 Al-Rubaiee, M., Yuan, B., Fan, Y., Zhu, S., Marsh, J. & Hou, L. Ultrastable 10 GHz Mode-Locked Laser on Semi-Insulating Substrate Through RF Injection Locking. *IEEE Photonics Technol. Lett.* (2024).
- 42 Hou, L. *et al.* Subpicosecond Pulse Generation at Quasi-40-GHz Using a Passively Mode-Locked AlGaInAs-InP 1.55- μ m Strained Quantum-Well Laser. *IEEE Photon. Technol. Lett.* **21**, 1731-1733 (2009).
- 43 Mercer, L. B. 1/f frequency noise effects on self-heterodyne linewidth measurements. *J. Lightwave Technol.* **9**, 485-493 (1991).
- 44 Zhao, Z. *et al.* Narrow laser-linewidth measurement using short delay self-heterodyne interferometry. *Opt. Express* **30**, 30600-30610 (2022).
- 45 Xu, Y. *et al.* Hybrid external-cavity lasers (ECL) using photonic wire bonds as coupling elements. *Scientific reports* **11**, 16426 (2021).

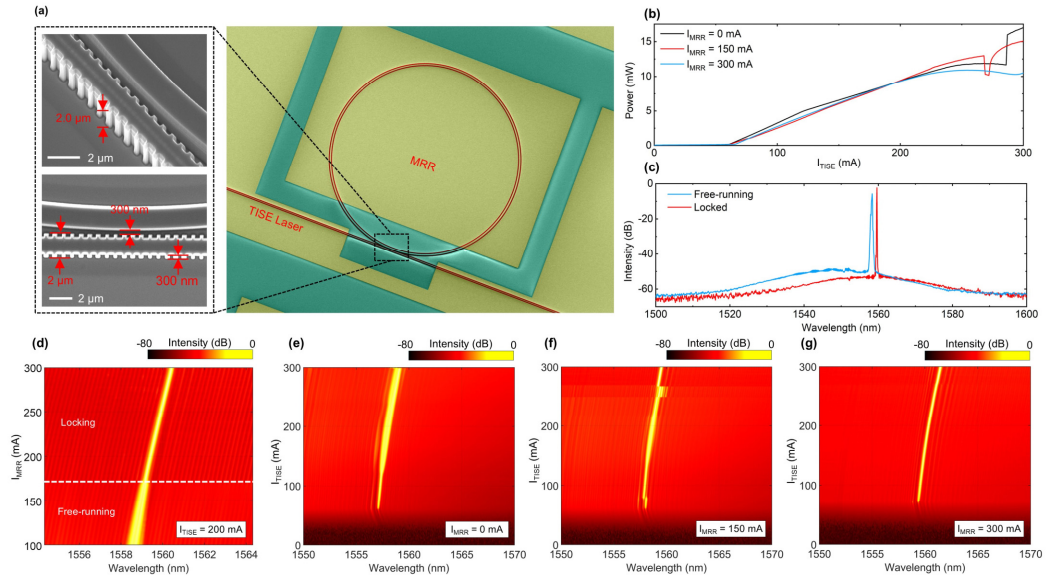
- 46 Wang, J. *et al.* Scalable single-microring hybrid III-V/Si lasers for emerging narrow-linewidth applications. *Opt. Express* **32**, 26751-26762 (2024).
- 47 Xiang, C. *et al.* Narrow-linewidth III-V/Si/Si₃N₄ laser using multilayer heterogeneous integration. *Optica* **7**, 20-21 (2020).
- 48 McKinzie, K. A. *et al.* InP high power monolithically integrated widely tunable laser and SOA array for hybrid integration. *Opt. Express* **29**, 3490-3502 (2021).
- 49 Zhu, Y. *et al.* Integrated Electro - Optically Tunable Narrow - Linewidth III - V Laser. *Adv. Photon Res.*, 2400018 (2024).
- 50 Han, M., Li, J., Yu, H., Li, D., Li, R. & Liu, J. Integrated self-injection-locked narrow linewidth laser based on thin-film lithium niobate. *Opt. Express* **32**, 5632-5640 (2024).
- 51 Larson, M. C. *et al.* in *Optical Fiber Communication Conference*. M2D. 1 (Optica Publishing Group, 2015).
- 52 Xu, Y. *et al.* Narrow-linewidth semiconductor laser with high-order sidewall gratings. *IEEE Photonics Technol. Lett.* **35**, 85-88 (2022).
- 53 Kumar, R. R. *et al.* A 10-kHz intrinsic linewidth coupled extended-cavity DBR laser monolithically integrated on an InP platform. *Opt. Lett.* **47**, 2346-2349 (2022).
- 54 Gaetano, E. D. & Sorel, M. Design of chirped-coupling sidewall Bragg gratings for narrow linewidth distributed feedback lasers. *Opt. Lett.* **44**, 1642-1645 (2019).

Fig. 1: Design of HF-OIL semiconductor laser



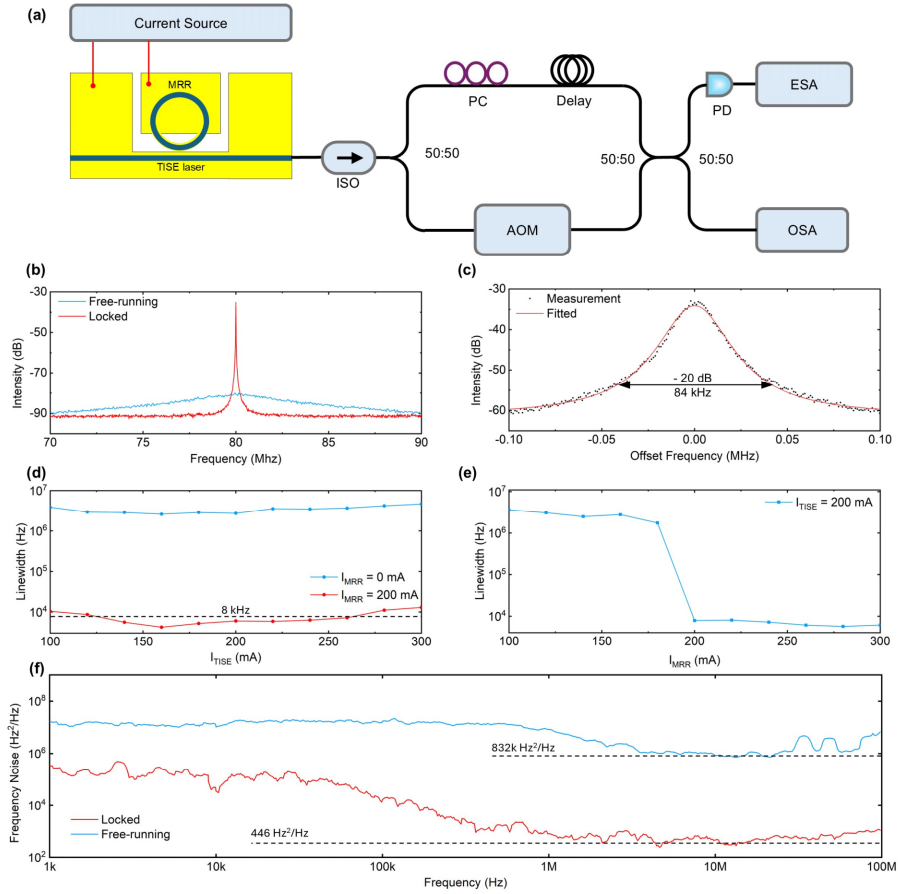
Structure and electrical field distribution of **a** traditional π -phase-shifted grating structure and **b** topological interface states extending (TISE) structure. **c** Modulation processing in TISE cavity including all the modulate periods. **d** Optical band structures of the left reflection grating (L_G), topological interface states extending (TISE) grating (L_M), and right reflection grating (L_{RG}). The left-side and right-side gratings have distinct Zak phases and the TISE range to form a Dirac cone dispersion at $k = 0.5$. **e** Schematic of the HF-OIL laser. **f** Schematic with structure dimension and electrical field distribution. **g** transmission spectrum and **h** normalized photon distribution in the TISE laser compared to the conventional π -phase shift DFB laser. **i** Transmission spectrum from the TISE laser to MRR.

Fig. 2: Device and spectrum narrowing



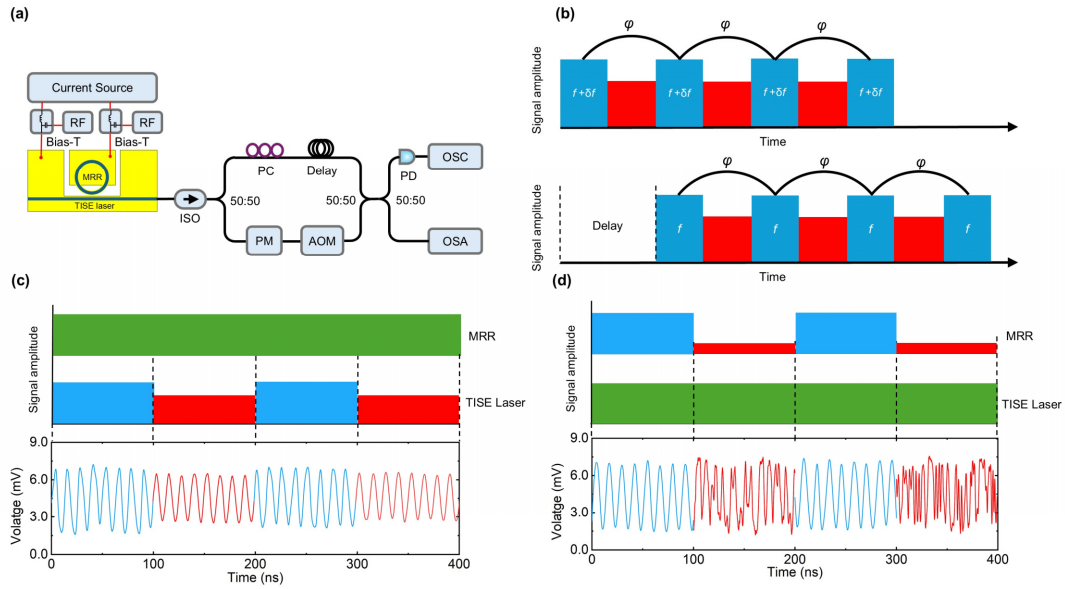
a SEM picture of the HF-OIL laser. **b** Typical I_{TISE} - P characteristics with different I_{MRR} . **c** Optical spectrum with the comparison of free running ($I_{MRR} = 0$ mA) and locking state ($I_{MRR} = 150$ mA), $I_{TISE} = 300$ mA. **d** 2D spectrum as a function of I_{MRR} with $I_{TISE} = 200$ mA. **e-f** 2D spectrum as a function of I_{TISE} with $I_{MRR} = 0$ mA, 150mA and 300 mA, respectively.

Fig. 3: Linewidth and phase noise



a Experimental setup: Light is collected from the TISE facet with a lensed fiber, and non-zero frequency self-heterodyne setup is used to measure the linewidth. ISO, isolator; AOM, acoustic-optic modulator; PC, polarization controller; PD, photodetector; ESA, electrical spectrum analyzer; OSA, optical spectrum analyzer; **b** Measured RF signal measured from PD with injecting locked $I_{MRR} = 200$ mA and $I_{TISE} = 160$ mA, yielding a dramatic narrowing of the emission linewidth compared to the free-running regime ($I_{MRR} = 0$ mA). **c** Voigt fitted linewidth with $I_{MRR} = 200$ mA and $I_{TISE} = 160$ mA. **d** linewidth as a function of I_{TISE} with $I_{MRR} = 0$ mA and 200 mA. **e** linewidth as a function of I_{MRR} with $I_{TISE} = 200$ mA. **f** Noise spectra of laser measured by correlated delayed self-heterodyne measurement between locked ($I_{MRR} = 160$ mA and $I_{TISE} = 200$ mA), and free-running signal ($I_{MRR} = 0$ mA and $I_{TISE} = 200$ mA).

Fig. 4: Injection locking phase encoding



a Experimental setup of the AMZI; PM, phase modulator; OSC, oscilloscope. **b** Principle of operation of the phase detection. **c** When the MRR operates in CW and is injected into the TISE laser, the TISE laser pulses all inherit the coherence. **d** When the TISE operates in CW and MRR switches from locking and free-running state, the TISE laser pulses switch between phase-locked and random state.